remote sensing

MDPI

Article

Impact of Base-to-Height Ratio on Canopy Height Estimation Accuracy of *Hemiboreal* Forest Tree Species by Using Satellite and Airborne Stereo Imagery

Grigorijs Goldbergs

Institute of Electronics and Computer Science, 14 Dzerbenes St., LV-1006 Riga, Latvia; grigorijs.goldbergs@edi.lv

Abstract: The present study assessed the large-format airborne (UltraCam) and satellite (GeoEye1 and Pleiades1B) image-based digital surface model (DSM) performance for canopy height estimation in predominantly mature, closed-canopy Latvian *hemiboreal* forestland. The research performed the direct comparison of calculated image-based DSM models with canopy peaks heights extracted from reference LiDAR data. The study confirmed the tendency for canopy height underestimation for all satellite-based models. The obtained accuracy of the canopy height estimation GeoEye1-based models varied as follows: for a *pine* (−1.49 median error, 1.52 m normalised median absolute deviation (NMAD)), *spruce* (−0.94 median, 1.97 m NMAD), *birch* (−0.26 median, 1.96 m NMAD), and *black alder* (−0.31 median, 1.52 m NMAD). The canopy detection rates (completeness) using GeoEye1 stereo imagery varied from 98% (*pine*) to >99% for *spruce* and deciduous tree species. This research has shown that determining the optimum base-to-height (B/H) ratio is critical for canopy height estimation efficiency and completeness using image-based DSMs. This study found that stereo imagery with a B/H ratio range of 0.2–0.3 (or convergence angle range 10–15°) is optimal for image-based DSMs in closed-canopy *hemiboreal* forest areas.

Keywords: digital surface model; base-to-height ratio; stereo; satellite; hemiboreal; canopy height

Citation: Goldbergs, G. Impact of Base-to-Height Ratio on Canopy Height Estimation Accuracy of *Hemiboreal* Forest Tree Species by Using Satellite and Airborne Stereo Imagery. *Remote Sens.* **2021**, *13*, 2941. https://doi.org/10.3390/rs13152941

Academic Editor: Lin Cao

Received: 20 June 2021
Accepted: 23 July 2021
Published: 27 July 2021

1. Introduction

The existence of forests is crucial for the well-being of people and the planet as a whole. Given the role of forests in the global carbon cycle and providing a wide range of ecosystem services, the ongoing assessment of forests' quantitative and qualitative state is critical [1]. Therefore, mapping and collecting precise and up-to-date data related to forest structure, biomass, species composition, and corresponding changes have become a mandatory part of forest management, inventories, and monitoring [2].

In Latvia, calculations of forest carbon stock changes and greenhouse gas (GHG) emissions are based on data provided by the National Forest Inventory (NFI) [3]. According to NFI data, forest covers 3.403 million hectares of land in Latvia, or 55% of the country's territory, the fourth-highest forest cover among all European Union (EU) countries. Since 2004, the Latvian NFI database, maintained by the Latvian State Forest Research Institute (LSFRI) "Silava", includes complete information related to Latvian forest stand parameters such as tree species, density, stock, forest stand height, biomass, etc., carried out at the plot level. However, traditional practices used for collecting this vegetation information are costly and time-consuming, providing low spatial coverage and requiring destructive fieldwork. Remote sensing complements traditional field methods through data analysis, enabling precise estimation of various forest inventory attributes across the high spatial range and different scales by avoiding destructive sampling and reducing time and cost from data acquisition to final output [4].

It is well known that canopy height, which correlated with other vegetation attributes, is an essential parameter for predicting regional forest biomass [5]. Thus, carbon accounting programs and research efforts on climate-vegetation interactions have increased the

demand for canopy height information. Worldwide, LiDAR (Light Detection And Ranging) data, combined with up-to-date advanced data processing methods, have proven to be efficient and precise tools for indirect fine-scale estimation of forest 3D structure parameters (primarily tree height) derived from high-density 3D point clouds [6]. Furthermore, by computing the difference between the canopy surface and the underlying ground, the calculated canopy height model (CHM) accurately reflects the spatial variations of the height of the canopy surface [7]. However, relatively high acquisition costs prevent airborne LiDAR from regularly mapping forest structural state and dynamics. Therefore, considering alternatives to airborne laser scanning (ALS) for continuous wide-area surveys, it is necessary to examine cost-effective approaches that use satellite data.

Higher temporal resolution, lower cost with broader area coverage, and spatially more homogeneous image content with multispectral information are the main advantages of satellite data over airborne remote sensing [8]. In the last decade, there has been growing interest in using very high resolution (ground sample distance (GSD) < 0.5 m) satellite-derived stereo imagery (VHRSI) to generate dense digital surface models (DSM) analogous to LiDAR data to support forest inventory and monitoring [9]. Structure from motion (SfM) and photogrammetric matching techniques [10,11] reconstruct the 3D object geometry and detect 3D coordinates by simultaneous matching of the same 2D object points located in overlapped stereo airborne and VHRSI imagery. However, while the ALS can penetrate the forest canopy and characterise the vertical distribution of vegetation, the VHRSI image-based point clouds only represent the non-transparent outer "canopy envelope" [9] or "canopy blanket" cover of dominant trees.

Most of the earlier studies regarding VHRSI image-based DSM performance used the plot-based approaches by deriving the main forest metrics such as the mean, maximum canopy heights, and height percentiles. Then, after performing regression with reference data (mostly LiDAR) and obtained estimation accuracy, the metrics are used as explanatory variables for predictive modelling of forest inventory attributes over certain areas. As an example, Grant D. Pearse et al. (2018) [12] compared point clouds obtained from Pleiades tri-stereo imagery to LiDAR data to predict *Pinus radiata* forest plot inventory attributes, such as mean height (R^2 = 0.81; RMSE = 2.1 m) and total stem volume (R^2 = 0.70; RMSE = 112.6 m^3 ha^{-1}). Additionally, L. Piermattei et al. (2019) [13] used Pleiades tri-stereo image-based CHMs to derive forest metrics in the Alpine region, compared to airborne image matching. Based on the applied pixel-wise approach, the forest metrics median errors −0.25 m (H_{max}), 0.33 m (H_p 95), −0.03m (H_{Std}) showed that satellite-based Pléiades CHMs could be an alternative to airborne images-derived CHMs in mountain forests. Based on calculated height metrics in 5-pixel samples, Neigh et al. (2014) [14] found IKONOS stereo imagery to be a useful LiDAR alternative for DSM calculation (R^2 = 0.84; RMSE = 2.7 to 4.1 m) in dense coniferous and mixed hardwood US forests. St-Onge et al. (2019) [15] successfully manually (RMSE = 0.9 m) measured individual tree heights in stereo mode using WorldView-3 imagery to predict basal area at tree and plot levels in sparse *Lichen* woodlands.

Several recent studies showed successful VHRSI image-based CHM performance connected to European boreal and hemiboreal forest tree species (*Scots pine*, *spruce* and *birch*). Persson and Perko (2016) [16] reported high correlations between WorldView-2 image-derived height metrics and reference LiDAR, with the estimation of Lorey's mean height with RMSE of 1.5 m (8.3%). The study identified the tendency to canopy height underestimation of dominant trees by using image-based CHMs. S.Ullah et al. (2020) [17] performed a plot-wise comparison of airborne, WorldView-2, and TanDEM-X image-based CHMs against field-based Lorey's mean and maximum height in a forest with pure, mixed pines and broadleaf tree species. This research confirmed that airborne stereo is the most accurate option (RMSE = 1.71 m, Lorey's mean height) compared to satellite-based models (RMSE = 2.04 m WorldView-2; RMSE = 2.13 m TanDEM-X).

Despite the large offer of VHRSI sensors on the market, image-derived DSM performance for retrieving the forest inventory data of different vegetation species in various

geographical regions is still not fully understood. Therefore, referring to the results of the remote sensing expert opinion survey performed by Fassnacht et al. (2017), the potential of VHRSI use for estimation forest attributes such as stand height is still unclear [18]. According to this survey, the mentioned reasons are a few studies and existing uncertainties associated with canopy height estimation accuracy.

Plot-wise approaches based on forest metrics have some limitations that sometimes restrict the comprehensive quantitative and qualitative performance evaluation of image-derived CHM models. First, most studies lack information related to image-based CHM completeness (percentage of detected canopy). Secondly, the height metrics do not directly estimate the outer "canopy envelope" DSM surface, which in most cases follows dominant treetops. It is also essential to recognise the differences in the DSM height estimates associated with different vegetation species. Thirdly, the accurate terrain layer (DTM) is needed to perform CHM creation.

Thus, the main objective of this study was to perform the direct comparison of calculated image-based DSM models with canopy peaks heights extracted from reference LiDAR data without canopy height model (CHM) generation. The present study assessed the airborne and satellite image-based DSM performance for canopy height estimation in predominantly mature, dense, closed-canopy Latvian *hemiboreal* forestland using forest inventory data.

To achieve this objective, the research: (1) evaluated and compared the vertical accuracy and completeness DSMs derived from stereo imagery of GeoEye1 and Pleiades1B satellites and large-format aerial UltraCam to reference LiDAR data; (2) analysed the differences in the DSM height estimates associated with different tree species; (3) examined the effect of sensor-to-target geometry (specifically base-to-height ratio) on matching performance and canopy height estimation accuracy; (4) investigated the satellite-based different spectral band DSMs performance on canopy height accuracy estimation.

2. Materials

2.1. Study Area

The "Taurkalne large forests" forestland area is located 100 km south-east of Rīga (56°30′ N, 25°00′ E), Latvia, Figure 1. The study area covers approximately 350 km^2, represented a relatively flat region with an elevation range varying between 40 and 80 m above sea level and mean annual rainfall of 690 mm. The selected territory represents a typical *hemiboreal* forestland pattern across the eastern part of Latvia with predominantly mature, dense, closed-canopy deciduous, and evergreen trees with some small open or grassy areas. The forest vegetation of the study site dominated by evergreen pine (*Pinus sylvestris*), spruce (*Pícea ábies*) and deciduous birch *(Bétula),* black alder (*Álnus glutinósa*) tree species. These tree species were the focus of this study.

2.2. Satellite and Airborne Data

In total, three sets of stereo imagery, acquired in the summer of 2020 by various optical satellites and airborne sensors, were used as the initial data in this study. The two in-track satellite imagery stereo pairs, GeoEye-1 (GE1) by *Digital Globe (USA)* and Pleiades1B by *Airbus Intelligence (EU)*, were obtained over the study area. The main characteristics of the imagery are given in Table 1 and Figure 2. Both imagery sets were provided altogether with rational polynomial coefficients (RPCs) data.

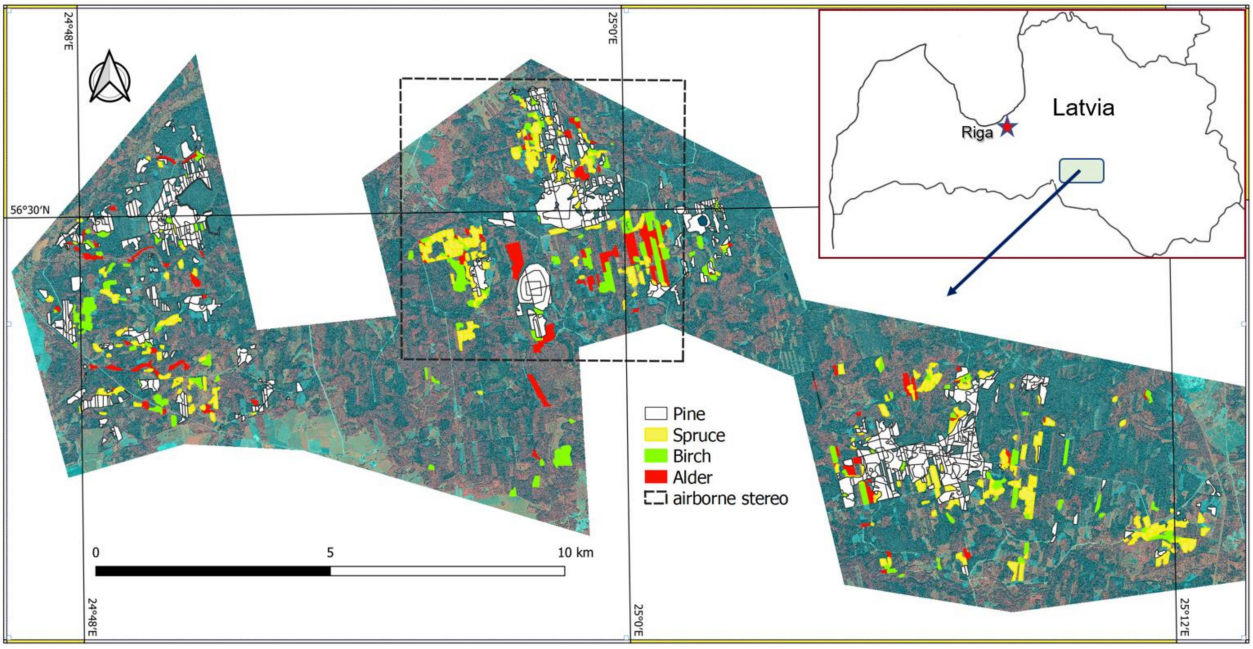

Figure 1. The 350 km^2 study area is represented by dense, closed-canopy deciduous, and evergreen forestland (GeoEye NIR-R-B orthophoto). The polygons represent the locations of chosen forests study plots, separated by four dominant tree species.

Table 1. Characteristics of stereo satellite imagery pairs (Pleiades and GE1) and airborne (UltraCam) acquired at the study site: PAN—panchromatic, R—red, G—green, B—blue, NIR—near-infrared sensor bands. All angles are given in degrees.

Sensor	Image ID	Acquisition Date/Time	Delivered Bands	Product GSD (m)	Convergence Angle	Base/Height Ratio	Sun Elevation/Azimuth
Pleiades	2020061309370 44-2020061309375 89	13 June 2020 12:37 p.m.	R,G,B,NIR	0.5 (pan-sharpened)	33.6	0.61	56.0/162
GE01	10500500ACDD9F00, 10500500ACDD9E00	7 August 2020 12:27 p.m.	PAN, R,G,B,NIR	0.5 2	14.7	0.28	48.5/159
UltraCam	80%/60% overlap	13 July 2020 9:30 a.m.	R,G,B,NIR	0.25	6.2/12.4	0.11/0.22	35/105

The radiometrically (16 bit GeoTIFF) and sensor-corrected GeoEye-1 *OrthoReady Stereo (OR2A)* processing level images were delivered. The GE1 imagery was projected to a plane using a Universal Transverse Mercator map projection and had no topographic relief applied, making them suitable for photogrammetric processing. Very high resolution (VHR) optical satellite Pleiades1B single pair (not tri-stereo) imagery, with 7% of cloud cover, was delivered with preserved true relief information (projected to a plane), radiometrically (12-bit JPEG2000), and sensor corrected. The cloud mask was automatically created and manually checked for further use in the given research. The vendor's pan-sharpening of Pleiades1B imagery resulted in a higher 0.5 m ground sample distance (GSD) spatial resolution of provided final 4-band (NIR-R_G-B) product.

To perform the complete research, additionally, twenty 4-band (NIR-R-G-B) aerial images with GSD resolution 0.25 m, acquired by *Georeal* company (Czech Republic) in July 2020 and provided by Latvian Geospatial Information Agency (LGIA), were used as a third imagery set. The images were taken at a flying height of 4600 m using UltraCam Eagle Mark 1, a frame large-format digital photogrammetric camera with a frame size of 13,080 × 20,010 mm and a focal length of 100.5 mm. The imagery formed a rectangular two strips block with 80% forward overlap and 35% side overlap. While the GE1 and Pleiades1B stereo satellite imagery sets fully covered the study area, the UltraCam airborne stereo imagery block had only 20% (70 km^2) coverage (Figure 1).

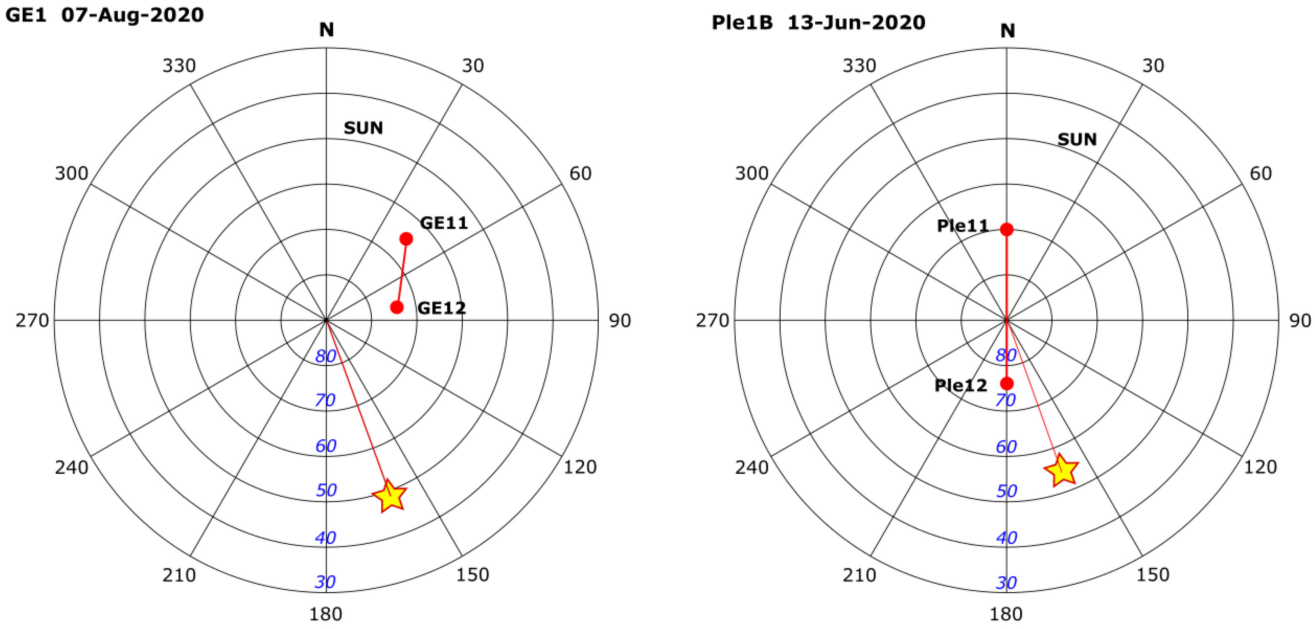

Figure 2. Polar diagrams of satellite stereo pairs: acquisition geometry describing the relative positions (elevation and azimuth angles) of the sun (yellow stars) and the sensors (red dots) to the target (circle centre). The given numbers of sensor positions (GE11, GE12, Ple11, Ple12), in each stereo pair, corresponding to acquisition time and catalogue order. All angles are given in degrees.

2.3. Reference Data

Airborne LiDAR and forest inventory (FI) data were used as reference data for this study. LiDAR open access data were acquired over the study area by MGGP Aero (Poland) at the end of May 2017 and provided by the Latvian Geospatial Information Agency (LGIA). The LiDAR data were collected with a Riegl LMS Q680i full-waveform sensor operating at a 400 kHz pulse repetition rate. An average flying height above ground level (AGL) was 800 m, scan angle 45 degrees, and flying speed of ~230 km/h. The average LiDAR point cloud density was more than 5 points per m^2. LiDAR data pre-processing, included data geo-referencing and point cloud classification, was performed with the *Terrasolid* software package by LGIA.

As LiDAR data acquisition time was three years before collecting stereo satellite data, the change detection related to forest clearcutting was performed across the study area. The clearcutting mask was created by using GE1, Pleiades, airborne orthophoto, and image-derived DSMs data. The automatically created polygons of the change detection mask were visually checked and manually corrected.

Forest inventory (FI) data were provided by the Joint Stock Company "Latvia's State Forests" (LVM) and included the forest plot complete metrics information, such as dominant and co-dominant tree species, species composition proportion, canopy height, age, density, estimated timber volume, etc. Across the study area, all FI plots were filtered and separated into four main tree species, based on the provided tree species composition coefficient. The plots with coefficient $\geq$7, meaning 70% of the dominant corresponding tree class in the given plot, were selected for this study. Finally, after applying the forest clearcutting mask, the forest plots with mature, dense, and closed-canopy forest cover were chosen (Table 2).

Table 2. Summary statistics of selected FI study plots, used in the given research and separated into four main dominant tree species.

Tree Species	No. Plots	Plots Area (ha)				Age (Years)	Height (m)
		Min	Max	Mean	Total	Mean	Mean
Pine (*Pinus sylvestris*)	688	0.14	25.68	1.77	1224	88	23
Spruce (*Pícea ábies*)	293	0.13	8.07	1.31	387	55	21
Birch (*Betula pendula*)	166	0.08	11.7	1.5	246	49	20
European black alder (*Álnus glutinósa*)	130	0.18	9.35	1.62	211	66	23

3. Methods

3.1. Data Processing Overwiew

The study performed the direct comparison of calculated image-based DSM models with canopy peaks heights extracted from reference LiDAR data, without canopy height model (CHM) generation (Figure 3). It was conducted in order to isolate one source of error uncertainty related to the accuracy of LiDAR DTM, generally used for CHM model calculation. The co-registration of the satellite imagery sets with LiDAR was performed during sensor orientation by GCPs measured and transferred from the LiDAR data. The main reason for the bias-compensated bundle adjustment using LiDAR GCPs was to minimise the image-based DSMs and LiDAR co-registration and geo-location discrepancies. Finally, we performed accuracy assessments related to image-derived DSMs performance in canopy height detection and estimation in open terrain and forest areas.

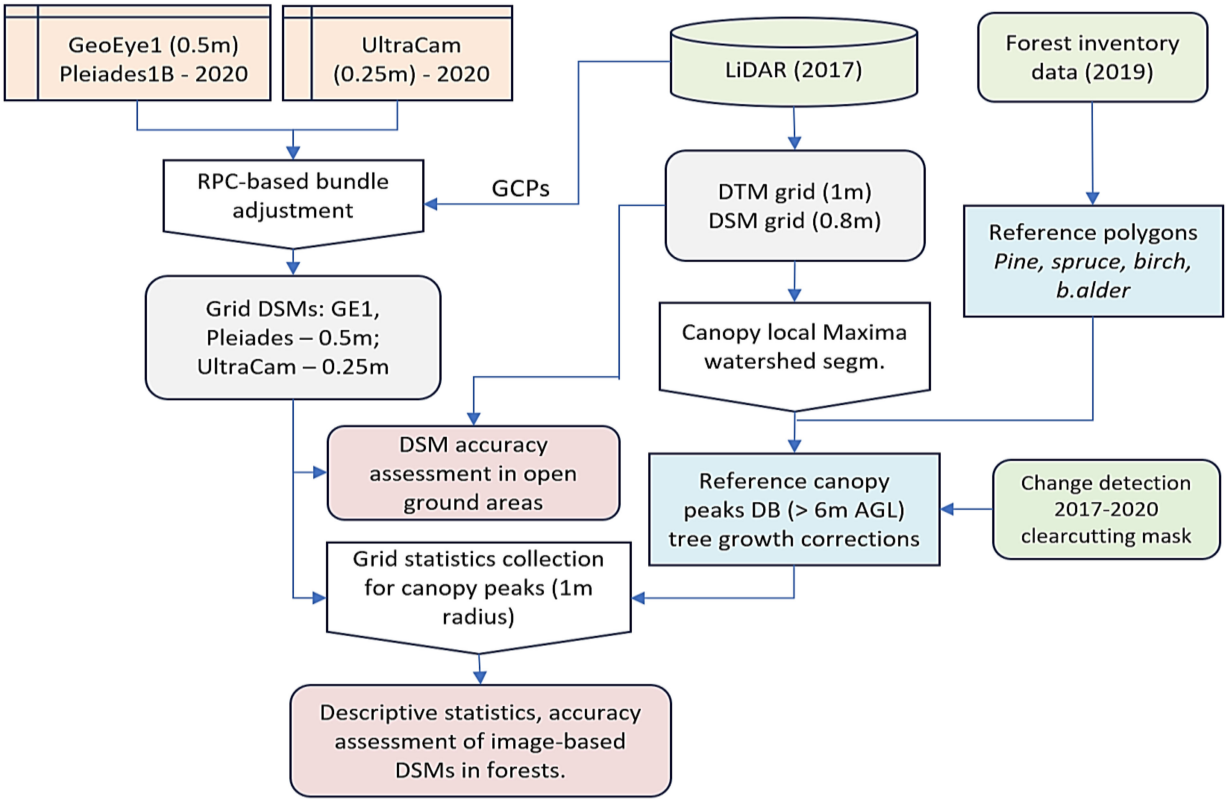

Figure 3. Workflow overview of a given study.

The software package *Photomod* v7.0 (Racurs, Moscow, Russia) was used for all photogrammetric image data processing steps, including imagery bundle adjustment and image matching DSM generation. All works related to LiDAR point cloud handling, such as DSM/DTM calculations and watershed segmentation routines, were carried out using

freeware *FUSION/LDV* v4.20 [19]. Grid DSMs comparison, corresponding grid statistics collection, and GIS-based analysis were performed using freeware SAGA GIS [20] and QGIS [21].

3.2. Sensor Orientation and Data Co-Registration

Image pre-processing started with pan-sharpening, applied to the GE1 imagery. The most robust enhanced principal component analysis pan-sharpening method was used, as it does not require radiometric correction.

External sensor orientation was performed with an empirical model based on rational functions with rapid positioning capability (RPC) data, refined by a zero-order polynomial adjustment. In general, it required just one ground control point (GCP) [22], and 4–5 well-distributed points would be recommended for a stereo pair to achieve the one-pixel accuracy [23,24] by using least-squares bundle adjustment. To achieve the best co-registration of the imagery with LiDAR, the eighteen (18) well-identified artificial GCPs (poles, concrete slab corners, road intersections) and well-identified natural (e.g., tree stumps) objects were transferred from the LiDAR data. The GCPs' height coordinates were extracted from the LiDAR, whereas their planar locations were manually identified in an existing orthophoto (0.25 m GSD) provided by LGIA.

All GCPs were well-distributed across the study area and manually measured by using stereo mode in *Photomod*. Fewer GCPs were used for geo-registration of the airborne UltraCam stereo imagery due to its partial coverage of the study area. The image geo-referencing accuracy and epipolar geometry of all imagery sets were improved by automatically measured tie points. The point measurements and bundle adjustment were performed once for every sensor (GE1, Pleiades, and UltraCam).

3.3. DSM Extraction from VHR Stereo Satellite Imagery and LiDAR Point Cloud

Five GE1 models (PAN, NIR, R, G, B) and five Pleiades1B models (NIR, R, G, B, NIR-G-B) were chosen for 0.5 m resolution grid DSM generation by using an SGM matching algorithm [10]. Additionally, two UltraCAM airborne imagery grid DSMs (NIR-G-B, 0.25 m resolution) with original in-strip overlap 80% and reduced overlap 60% were extracted. The two UltraCam models with different overlap settings were selected to investigate the effect of the base-to-height ratio on generated DSM accuracy. Altogether, twelve grid DSM models were used in the further analysis.

After testing various SGM settings, the following slightly modified *Photomod* SGM default settings were used for image-based DSM calculations: census transform (CT) matching cost function with pixel cost calculation radius 3 and eight calculation paths; decreased penalty value 4 for parallax changes by one pixel and a reduced penalty value 80 for parallax change by more than one pixel. No filters were applied on generated DSM models, except median filter with mask aperture (7 pixels) and threshold (1 m) to recalculate low-correlated "noisy" pixels along feature edges (e.g., forest borders), keeping rest values unchangeable. To fill the gaps (null cells) that appeared on DSMs due to occlusions and bad imagery textures, the SAGA GIS "stepwise resampling" tool was applied using a *B-spline* interpolation algorithm with grow factor 2.

3.4. Accuracy Assessment of the Image-Based DSMs in Open Ground Areas

Although imagery was vertically co-registered with LiDAR during sensor orientation, the extracted DSMs got a unique vertical bias. Thus, the vertical DSM offset from one to another and LiDAR surface must be calculated before their elevation comparison and final accuracy assessment. Firstly, the 1 m resolution grid DTM from LiDAR dense point cloud was created by assigning the mean elevation of ground classified returns within each grid cell. The created grid LiDAR DTM played as ground truth for further vertical accuracy assessment of the image-based DSMs in selected open ground areas. The corresponding open ground areas were chosen manually using a visual examination of LiDAR, satellite imagery and orthophoto maps to avoid altered and overgrown grass and shrubs. Alto-

gether, the 134 open ground polygons (plots) were manually digitised with a mean of 0.9 ha and a total area of 120 ha, well-distributed across the study area. Within this created open ground mask, the image-based DSM ground surfaces were aligned to those of the reference LiDAR-based DTM. As image-based DSMs had higher resolution than 1 m LiDAR DTM, the mean height values of the pixels that are in the cell of LiDAR DTM were chosen. After the pixel-wise ground surfaces comparison, the obtained vertical offsets were applied to all image-based DSMs values for further accuracy assessment in forest areas.

3.5. Accuracy Assessment of Image-Based DSMs in Forest Areas

To perform the quality and efficiency assessment of image-based DSM in selected forest areas, the reference heights of individual canopy peaks were extracted from LiDAR data. To do this, the local maxima approach by using watershed segmentation was used for individual canopy peaks detection and extraction from the LiDAR grid DSM. First, the DSM was interpolated from the LiDAR dense point cloud using the "CanopyModel" routine in *Fusion*. Based on LiDAR point cloud density quantity, the optimal grid DSM with 0.8 m pixel resolution was generated by assigning the highest return of the LiDAR point cloud within each grid cell. A median convolution smoothing filter with a 3×3 window was applied on the generated DSM. The *Fusion* 'peaks' switch was used to preserve the localised elevation peak (local maxima) values from the filtering. Secondly, the *Fusion* "TreeSeg" watershed segmentation algorithm was applied to a LiDAR-based DSM to produce segments representing individual canopy peaks. As a result, the calculated high point list, including the heights and locations of individual canopy peaks, was created in shapefile format.

The obtained canopy peaks list was filtered using selected forest inventory study plots polygons (Table 2) and separated into four main dominant tree species. To compensate for the changes in canopy heights due to trees growing in time between LiDAR data (2017) and satellite imagery (2020) acquisitions, the extracted LiDAR canopy peaks heights were adjusted based on each tree species annual growth rate. The trees annual growth rates values were obtained from the Latvian State Forest Service and published by LSFRI "Silava' [25]. The canopy peaks list was finalised by excluding all height values less than <6 m above ground by performing GIS analysis after assigning ground height attribute from earlier generated LiDAR grid DTM.

The quality and accuracy assessment of the image-based DSMs in selected forest areas was assessed in two ways: vertical accuracy and completeness. The vertical accuracy assessment was performed by comparing the image-based DSM grid height values with corresponding individual canopy peaks (height maxima) extracted from reference LiDAR data. It was conducted by collecting height metrics statistics of image-based DSM pixel values within a 1 m radius surrounding every appropriate LiDAR-based canopy peak (Figure 4). The highest DSM grid height value of the surrounding 13 pixels (within 1 m radius) per canopy LiDAR height peak was selected and compared.

To perform the canopy completeness (detection) and vertical accuracy assessments, all heights of image-based DSM grid cells assigned to LiDAR individual canopy peaks were filtered. First, all image-based DSM heights less than <2 m above ground, were marked as non-detected canopies and excluded from the final assessments. This GIS-based filtering of image-based DSM heights was performed by canopy height calculation using ground height values extracted from corresponding LiDAR grid DTM. Secondly, all measurements with height differences more than >20 m between corresponding image-based DSM heights and LiDAR peaks were marked as outliers and excluded from the final assessments. Thus, the final completeness of the image-based DSMs was assessed as the proportion of the number of LiDAR local canopy peaks with assigned image-based DSM heights (H_{canopy} > 2 m) with removed outliers to the total number of extracted LiDAR canopy peaks. Finally, the descriptive statistics and linear regression were calculated for all compared DSM and LiDAR heights in every model for each tree species.

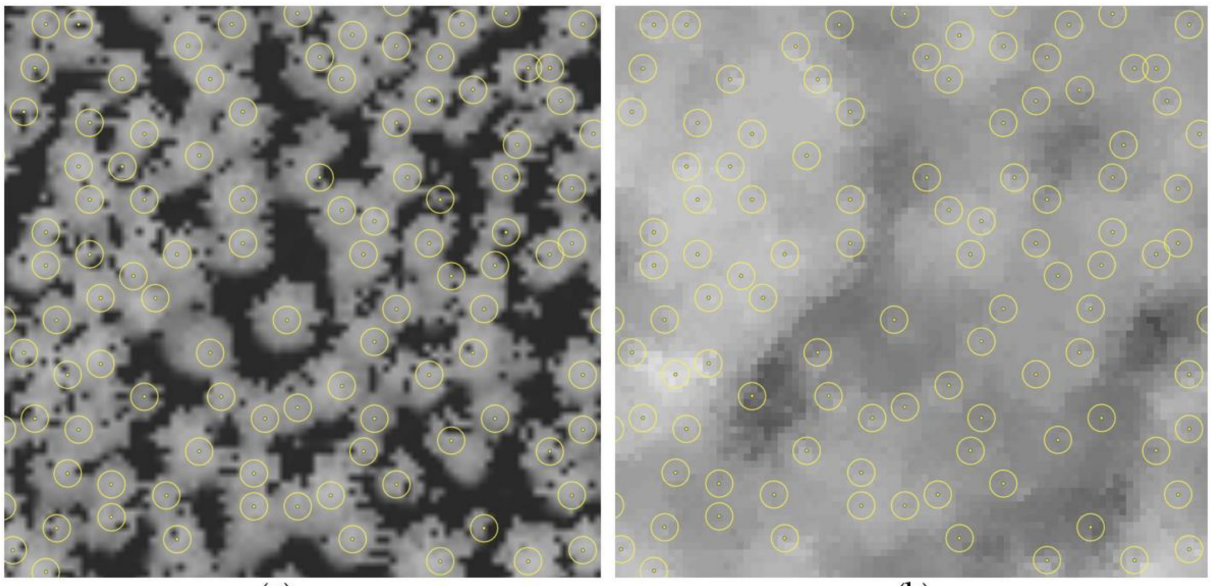

Figure 4. DSM fragments 40 × 40 m of the study area. *Spruce* canopy peaks (yellow dots) extracted from LiDAR-based DSM (**a**) by local maxima approach with 1 m radius (yellow circles) for collecting grid statistics (heights) from image-based DSM (**b**). The GE1-PAN DSM (**b**) represents the non-transparent outer "canopy envelope" or "canopy blanket" cover of dominant trees compared to LiDAR-based DSM (**a**).

For all statistics measurements, the normalised median absolute deviation (NMAD) was used, Equation (1), where: Δh_j denotes differences between reference (LiDAR) and extracted DSM cell (j) values, and m—median quantile of the differences:

$$\text{NMAD} = 1.4826 * median_j\left(\left|\Delta h_j - m_{\Delta h}\right|\right) \quad (1)$$

The NMAD is an accuracy measure more suited for photogrammetry-derived and cloud-based DEMs as it is more resilient to outliers than standard deviation [26].

4. Results

4.1. Accuracy of the Sensor's Stereo-Pair Orientation

The satellite and airborne stereo-pairs orientation results are based on rational functions with RPC data and least-squares bundle adjustment and root mean square errors (RMSE) on GCPs, shown in Table 3. The sub-pixel imagery orientation accuracy was achieved in every sensor model. The geo-positioning accuracy of the Pleiades imagery was the least accurate due to radiometric and geometric differences of the Pleiades and GE1 imagery, impacting on non-signalised GCPs identification and measurements. At the same time, the vertical sensor orientation accuracy of Pleiades imagery was 50% higher than in the GE1 case due to the higher Pleiades base-to-height ratio parameter [27].

Table 3. Bundle adjustment results of the imagery orientation based on GCP measurements (root mean square errors (RMSE)) of three stereo imagery sets: satellites imagery of GeoEye1, Pleiades, and airborne UltraCam.

Stereo Pair	Nr. GCPs	RMSE X (m)	RMSE Y (m)	RMSE Z (m)
GeoEye1	18	0.31	0.35	0.33
Pleiades	18	0.45	0.42	0.21
UltraCam	6	0.19	0.16	0.18

4.2. Accuracy of the Image-Based DSMs in Open Ground Areas

The results obtained from the pixel-wise comparison of the image-derived DSM-based ground surfaces with extracted LiDAR DTM are presented in Table 4, Figure 5. The table provides only spectral models with the best results (lowest RMSE) as the rest showed almost identical output.

Table 4. Pixel-wise comparison of the image-based (DTM_{SGM}) and LiDAR (DTM_{LiDAR})-ground surfaces, based on corresponding elevation cell descriptive statistics (in metres), where: UltraCam 60—model with in-strip 60% imagery overlap, UltraCam80 with in-strip 80% overlap. Negative values represent an underestimation.

DTM_{SGM}–DTM_{LiDAR}	GE1-PAN	Pleiades-NIR	UltraCam60	UltraCam80
No. of comp.pixels	1,107,080	1,056,289	137,976	137,976
Mean (m)	0.08	−0.04	0.03	0.01
Median (m)	0.10	−0.04	0.01	0.03
RMSE (m)	0.54	0.33	0.40	0.41
NMAD (m)	0.61	0.31	0.38	0.46

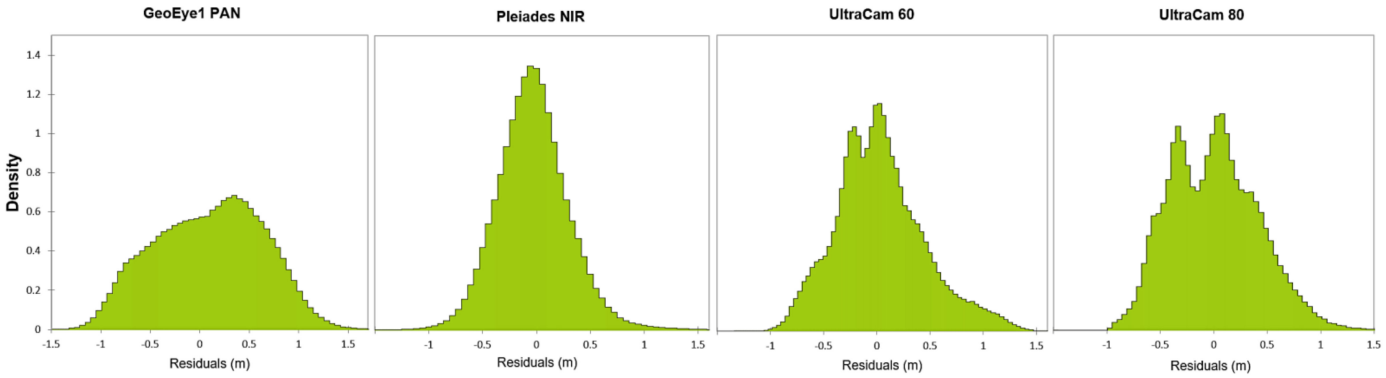

Figure 5. Error distribution histograms of ground surface pixel-wise comparison of the corresponding image-based (DTM_{SGM}) and LiDAR (DTM_{LiDAR}) models.

Overall, these results indicate that sensor orientation and image-derived DSM co-registration based on transferred LiDAR GCPs were conducted accurately and adequately. The most noticeable finding to emerge from these results is that Pleaides-based DSM demonstrated the highest accuracy of open ground surface detection. The reason for this is most likely in the higher base-to-height ratio of Pleiades imagery. The most surprising aspect of the results is the lower accuracy (RMSE) of airborne-based UltraCam DSM ground surfaces than the Pleiades. A possible explanation for this might be that the geospatial resolution of UltraCam imagery is twice higher than satellite data, also providing more detailed information in a vertical plane with higher variance in vertical error distribution. No significant differences were found in ground detection accuracy between two UltraCam-derived DSM models related to using all (80% overlap) and a reduced number (60% overlap) of images.

4.3. Completeness and Vertical Accuracy of Image-Based DSMs in Forest Areas

The vertical accuracy assessment of image-based DSMs in selected forest areas (Table 2) were based on comparison with heights of individual canopy peaks ($H_{canopy} > 6$ m) of reference LiDAR data, and are shown in Table 5, Figure 6. From a total of twelve analysed image-based DSMs, only seven are presented in Table 5 and Figure 6: three GeeoEye1 DSMs (PAN, best spectral, worst spectral), two Pleiades (best/worst single spectral DSM), and two UltraCam (with 80% overlap and reduced number 60% overlap). The best/worst models were filtered based on median (50%) error and lowest RMSE/NMAD values.

Table 5. Descriptive statistics of vertical accuracy assessments of image-derived DSMs compared to the LiDAR individual canopy peaks and separated by four main vegetation species, where GE1—*GeoEye1*, Ple—*Pleiades1B*, *Ucam*—UltraCam-based models, PAN—panchromatic and NIR—near-infrared, etc. Values are in metres, except completeness (%). Negative values represent an underestimation of image-derived DSMs. The UltraCam images had a smaller coverage of the study area.

Pine (*Pinus sylvestris*)							
DSM_{SGM}−$LiDAR_{tree\_peaks}$	**GE1-PAN**	**GE1-BLUE**	**GE1-RED**	**Ple-NIR**	**Ple-RED**	**Ucam 80**	**Ucam 60**
No. of detected peaks	552,779	553,027	550,874	410,193	345,700	163,193	157,368
Completeness (%)	98.4	98.4	98.0	73.1	61.6	98.9	99.0
Linear regr. R^2	0.96	0.96	0.96	0.89	0.85	0.97	0.97
Mean	−1.34	−1.32	−1.45	−2.41	−2.84	−1.19	−0.93
Median (50%)	−1.51	−1.49	−1.61	−1.90	−1.99	−1.38	−1.20
RMSE	2.28	2.30	2.34	3.83	4.44	1.76	1.75
NMAD	1.52	1.53	1.57	1.97	2.10	1.25	1.12
Spruce (*Pícea ábies*)							
DSM_{SGM}−$LiDAR_{tree\_peaks}$	**GE1-PAN**	**GE1-BLUE**	**GE1-NIR**	**Ple-GRN**	**Ple-RED**	**Ucam 80**	**Ucam 60**
No. of detected peaks	201,254	201,234	201,250	191,615	190,104	82,062	79,872
Completeness (%)	99.6	99.5	99.5	94.8	94.0	99.6	99.6
Linear regr. R^2	0.92	0.92	0.92	0.85	0.85	0.91	0.92
Mean	−0.94	−0.93	−1.07	−1.81	−1.95	−0.50	−0.39
Median (50%)	−0.95	−0.94	1.07	−1.44	−1.53	−0.56	−0.44
RMSE	2.40	2.42	2.49	3.34	3.38	1.85	1.76
NMAD	1.97	1.97	2.07	2.31	2.34	1.66	1.47
Birch (*Betula pendula*)							
DSM_{SGM}−$LiDAR_{tree\_peaks}$	**GE1-PAN**	**GE1-BLUE**	**GE1-NIR**	**Ple-BLUE**	**Ple-RED**	**Ucam 80**	**Ucam 60**
No. of detected peaks	129,198	129,170	129,068	119,133	119,104	52,446	43,045
Completeness (%)	99.3	99.3	99.2	93.3	91.8	99.7	99.5
Linear regr. R^2	0.92	0.92	0.91	0.86	0.85	0.87	0.90
Mean	−0.25	−0.26	−0.32	−0.88	−1.00	−0.20	−0.34
Median (50%)	−0.26	−0.27	−0.31	−0.60	−0.72	−0.14	−0.26
RMSE	2.55	2.56	2.60	3.36	3.35	2.21	2.02
NMAD	1.96	1.97	2.01	2.15	2.16	1.60	1.25
European black alder (*Álnus glutinósa*)							
DSM_{SGM}−$LiDAR_{tree\_peaks}$	**GE1-PAN**	**GE1-BLUE**	**GE1-RED**	**Ple-GRN**	**Ple-NIR**	**Ucam 80**	**Ucam 60**
No. of detected peaks	120,767	120,744	120,749	119,666	119,567	68,934	57,471
Completeness (%)	99.9	99.9	99.9	99.0	98.9	99.7	99.8
Linear regr. R^2	0.91	0.91	0.90	0.86	0.85	0.88	0.89
Mean	−0.06	−0.07	−0.13	−0.51	−0.64	0.16	0.11
Median (50%)	−0.31	−0.32	−0.38	−0.53	−0.58	−0.02	−0.04
RMSE	2.55	2.56	2.59	3.10	3.20	2.05	1.87
NMAD	1.52	1.52	1.55	1.83	1.86	1.21	1.07

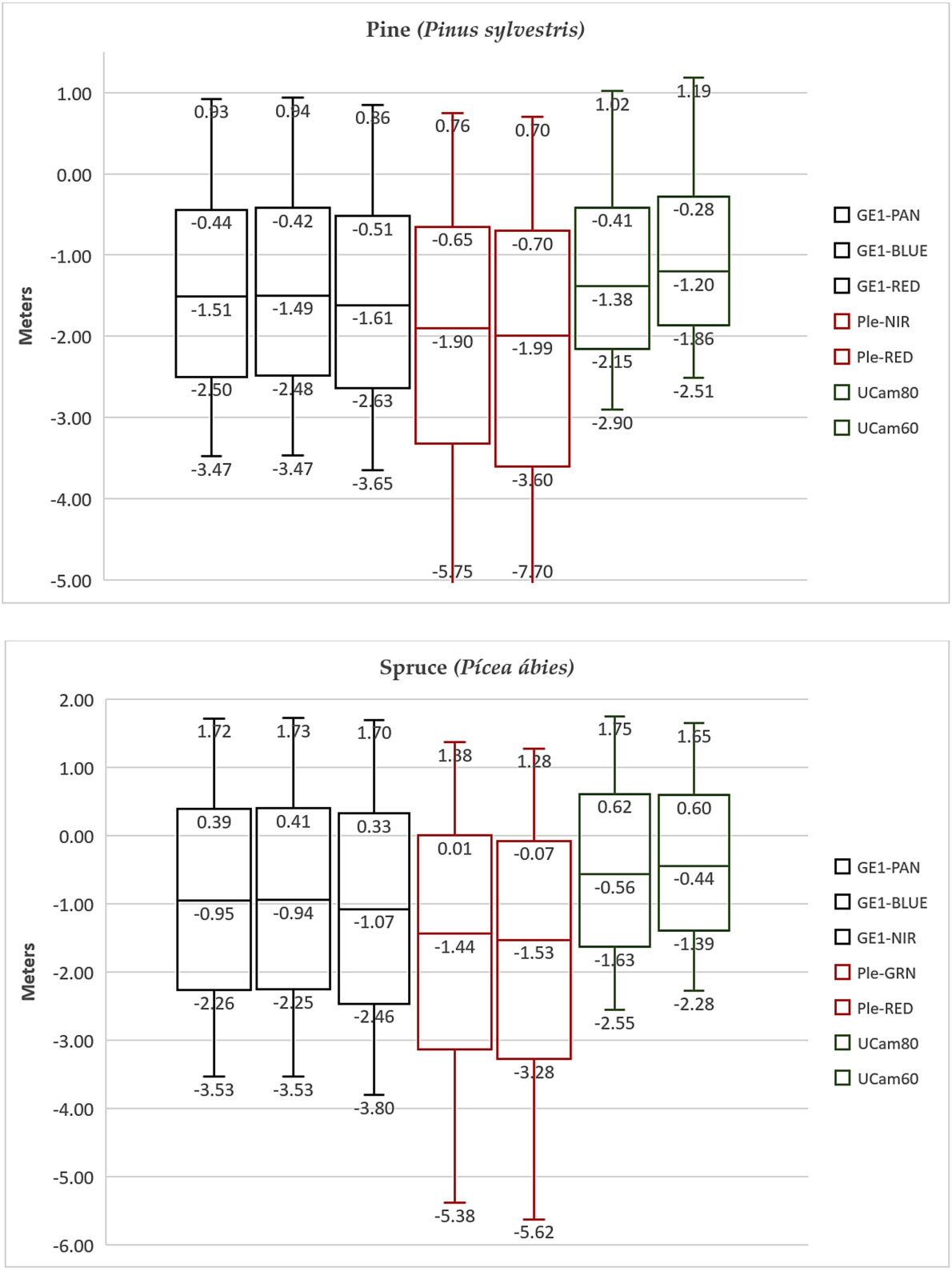

Figure 6. *Cont.*

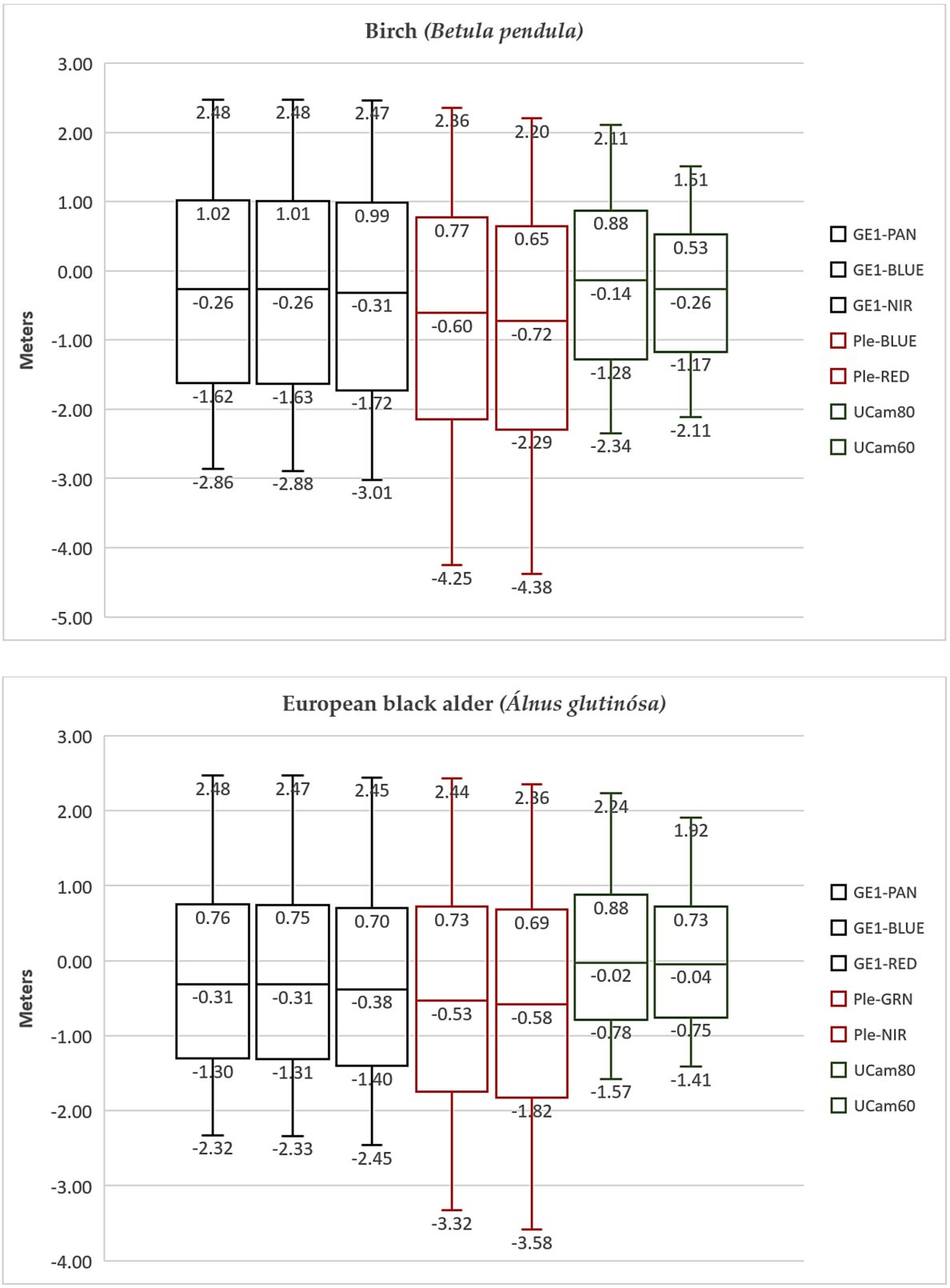

Figure 6. The accuracy box plots represent differences between image-derived DSMs heights and corresponding LiDAR individual canopy peaks in selected models (X-axis) and separated by four main vegetation species, where: vertical boxes represent the errors range (Y-axis, meters) between the lower (Q_1 = 25%) and higher (Q_3 = 75%) quartiles; the lower/higher whiskers are 10% and 90% percentiles; the horizontal line in the box is the median error (50%); GE1 = *GeoEye1*; Ple = *Pleiades*; UCam—*UltraCam (80% and 60% overlap)* based models with sensor band accordance.

These results indicate an essential connection between the image-derived DSM canopy height accuracy, canopy completeness, and corresponding vegetation tree species. The Figure 7 summarises all previously given results based only on one best model per sensor and two accuracy measures: median error and NMAD. All image-based DSMs show underestimation in height detection for all tree species, except *black alder*, using the airborne UltraCam sensor. Coniferous trees (*pine*, *spruce*) are less accurate in height estimation and have a higher error variance than deciduous tree species (*birch*, *black alder*). Comparing the image-based DSMs results of two used satellites reveals that all GeoEye1 DSMs provided higher results in dense forest canopy detection and height accuracy estimation than Pleiades1B models. The best outcome was achieved by using airborne UltraCam imagery with 60% in-track overlap. The possible reasons for the given consequences are discussed in the forthcoming section.

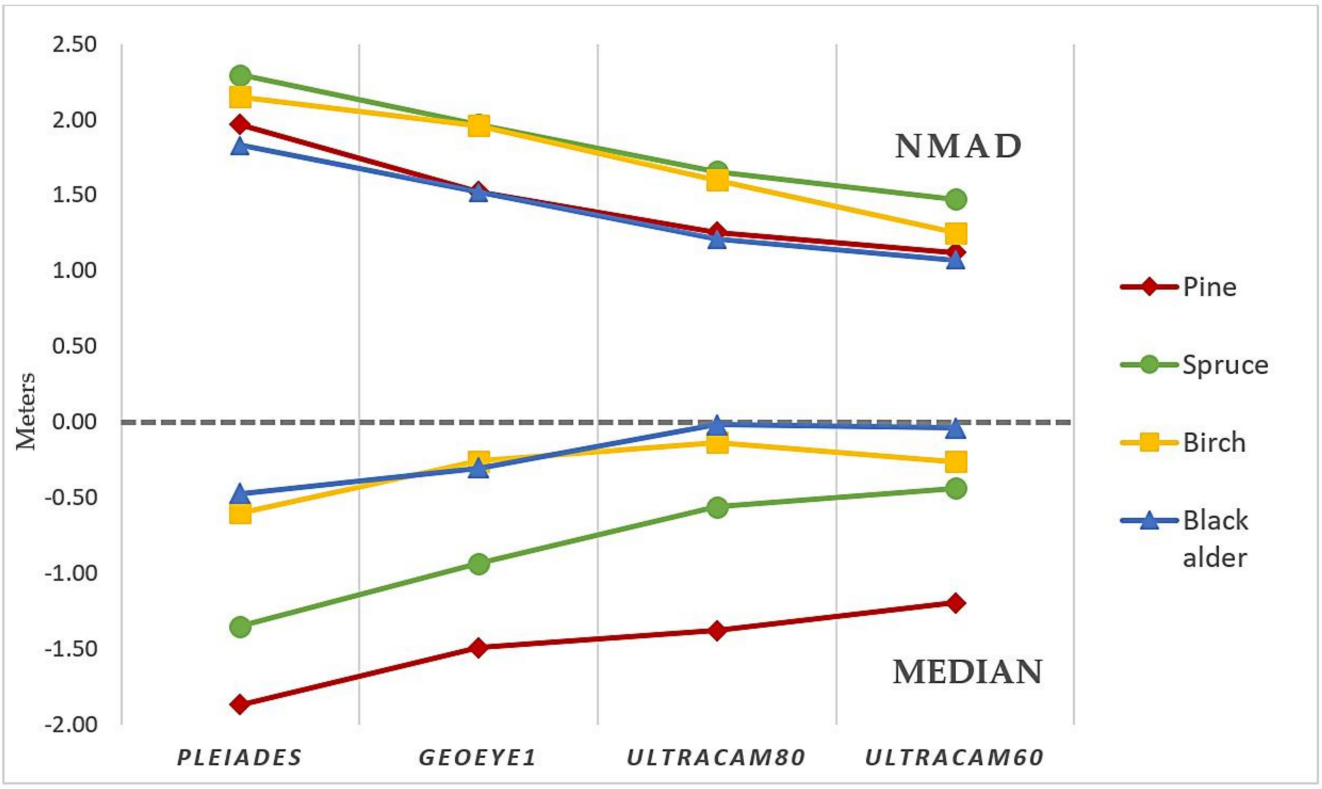

Figure 7. The Summary statistics of the best image-derived DSMs compared to the LiDAR individual canopy peaks, based on two vertical accuracy measures (median error and NMAD) and separated by four main vegetation species. Values are in metres. Negative values represent an underestimation of image-derived DSMs.

5. Discussion

In total, the vertical accuracy and completeness of image-based DSMs are affected by the base-to-height ratio parameter, the canopy vegetation vertical structure, species composition, image band radiometry, sensor-to-target and sun-to-sensor geometry, wind, and other minor factors [28]. The ability to identify or distinguish canopy or its parts based on light scattering and reflection differences is the key to the success of image matching techniques. Sufficient image contrast and brightness between neighbour objects surfaces (e.g., between two crowns; crown and ground) can improve the matching performance and, therefore, crown/canopy detection rate and height accuracy. The current study found that the base-to-height ratio of stereo imagery geometry was the critical factor influencing image-based DSM performance. In our research, the sun-to-sensor viewing geometry was similar for GE1 and Pleiades1B satellite sensors. Therefore, the discussion is mainly focused on sensor-to-target geometry and does not provide a detailed understanding of how the

changes in sun-to-sensor geometry (e.g., sun elevation and azimuth angles) influence canopy surface estimates by image-based DSMs.

5.1. Vertical Accuracy of Image-Based DSMs in Open Ground Areas

This study results confirmed the previous findings [27,29] that satellite imaging geometry, particularly the base-to-height (B/H) ratio related to stereo-pair convergence angle, plays a substantial role in the completeness and vertical accuracy of image-derived DSMs. In our study, the Pleiades-based DSMs, with the highest B/H ratio of 0.61, showed the highest performance and accuracy in height estimation of open ground areas. It is somewhat surprising that Pleiades pan-sharpened imagery (0.5 m GSD) was more efficient in open terrain detection than airborne UltraCam images with a 0.25 m resolution. Only Pleiades models achieved the sub-pixel vertical accuracy with RMSE 0.33 m and NMAD 0.31 m, showed a Gaussian error distribution pattern (Figure 5). Another proof of *Pleiades* imagery high performance in open ground detection is the sensor's orientation results (Table 3). Despite worse *Pleiades* planimetry accuracy than GE1 and UltraCam, the achieved vertical accuracy based on GCP measurements was 1.5 higher than GE1 and almost the same as UltraCam. Since GCP measurements for sensor bundle adjustment were carried out manually in stereo mode, this also allows me to recommend using imagery with a high B/H ratio for manual stereo restitution of open terrain areas and artificial objects with continuous and solid surfaces. There was an insignificant discrepancy in performance between different spectral band-based DSM models of the same corresponding sensor. Taken together, the findings from this study suggest that stereo imagery with B/H ratio > 0.5 (or convergence angles > 30°) preferably have to be used for DSM creation in open ground areas with flat terrain patterns. This conclusion agrees with the findings of other studies [27,29,30], in which the per-point vertical accuracy of image-based DSMs in open-ground areas directly correlates with increasing B/H ratio or convergence angle.

5.2. Completeness and Vertical Accuracy of Image-Based DSMs in Forest Areas

Opposite results were achieved in forest areas related to tree height estimation and completeness, where all Pleiades-based DSM models were worse than GE1 and even more so than UltraCam (Table 5, Figure 6). The completeness of pine (*Pinus sylvestris*) of Pleiades NIR-based DSM was 25% less (73%) than GE1 DSM performance (98%) and almost half-meter more in canopy height underestimation. In addition, all Pleiades DSM models showed a higher error variance (RMSE, NMAD) than other sensor-based DSMs, noticeably below the first quartile (25%) of the errors. The main reason for this outcome is directly related to the stereo imagery geometry, namely the B/H ratio or stereo-pair convergence angle.

The dense closed-canopy forest areas with near-continuous tree cover are characterised by the high surface roughness of different tree shapes. Therefore, the detection efficiency of every part of the canopy depends on the viewing directions of the stereo pair, namely, on how accurately and correctly the same part of the rough canopy surface will be displayed on the images. In forest areas, crown shape and tree structure that strongly influence the sun's reflection come out in the first place [31]. For trees with a conical crown shape, a large convergence angle may lead to a situation where the same part of the canopy may be wrongly displayed on one image due to poor reflection towards the sensor or invisibility (occlusion). The high B/H image ratio creates large parallax for high-rise crowns (canopies), increasing areas that cannot be matched correctly due to occlusions. Furthermore, during image matching, the mismatch of the same feature often leads to wrong height calculations and incomplete DSM [32]. As a result, for trees with conical (tapering) crown shapes, canopy height underestimation is expected and exists. Depending on tree species, the canopy height underestimation in dense closed-canopy forests can reach up to several meters, or 8% of mean canopy height (e.g., *pine* in the Pleiades case).

Broadleaf deciduous tree species increase the sun reflectance by reducing tree crown transparency, smoothing the top of the canopy shape's roughness, and increasing the

reflection area. As a result, the image-based DSMs of forests with dominated broadleaf species (e.g., *birch* and *black alder*) show higher efficiency and accuracy in canopy height estimation and completeness (Figure 7).

Based on the results of this study, it can be concluded that the presence and variability of the types of canopy surfaces negate the advantage of a large convergence angle use, leading to a decrease in SGM matching performance (Pleiades case). This finding corroborates the recent research of Rongjun Qin (2019) [33], which suggested that a smaller convergence angle (can be as small as around 7°) yields better results for dense surface reconstruction and complete DSM in urban areas.

Summarizing the results of this study, it is possible to construct a relationship between the obtained efficiency (vertical accuracy and completeness) of image-based DSMs and the base-to-height (B/H) ratio of corresponding imagery in *hemiboreal* predominantly mature, dense, closed-canopy forestland (Figure 8). However, this graph must be interpreted with caution because we omitted the effect of sun-to-image geometry, which was almost the same for satellite-based sensors in this study, and resolution differences between satellite and airborne imagery. It should also be borne in mind that the convergence angle in the case of frame aerial imagery is variable over the entire overlap of each stereo model. In most cases depend on the location on a stereo model, the convergence angle is less than the nominal values calculated based on the B/H ratio, Table 1. Based on airborne imagery performance, further research should be conducted in order to investigate the efficiency of satellite stereo imagery with the B/H ratio range between 0.15 and 0.25 (e.g., Pleiades tri-stereo approach) in similar forest areas. Overall, this study suggests that stereo imagery with a B/H ratio range of 0.2–0.3 (or convergence angle range 10–15°) is optimal for image-based DSMs in closed-canopy *hemiboreal* forest areas.

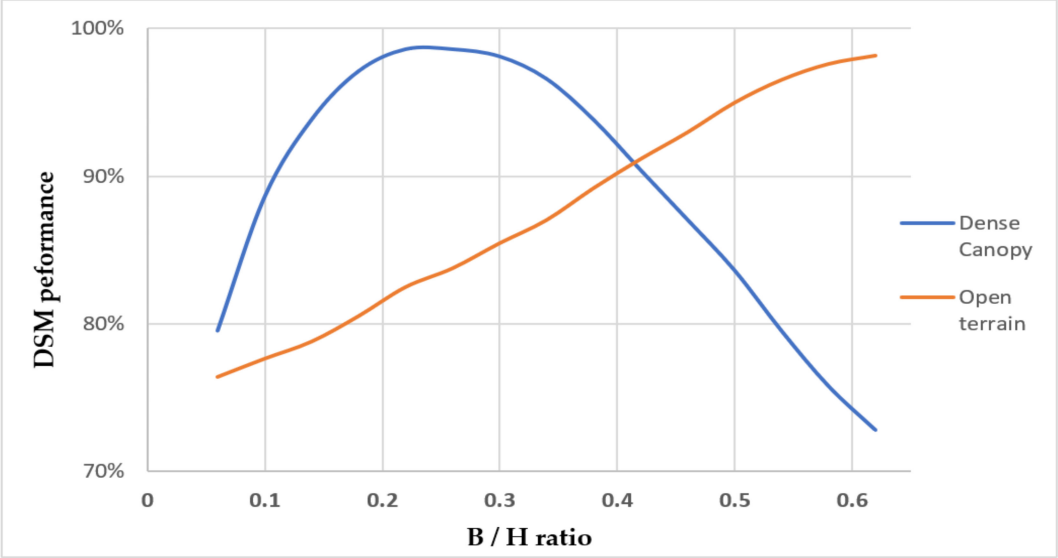

Figure 8. Relationship between the efficiency (vertical accuracy and completeness) of image-derived DSMs and base-to-height (B/H) ratio of corresponding stereo satellite and airborne imagery in *hemiboreal* predominantly mature, dense, closed-canopy deciduous and evergreen forestland.

To improve the performance of semi-global matching, the research also checked the efficiency of SGM matching settings by aggregating the cost along 16 paths instead of 8 (used in given research). The results showed a variable difference in accuracy with no significant improvements and a substantial calculation time increase. Moreover, the gains by using 16 paths were only noticeable for dominant stand-alone trees or groups of trees, which were out of the given study objectives.

5.3. Vegetation Reflectance and Image-Based DSM Performance

Besides the base-to-height ratio, the canopy detection performance also depends on how a vegetation surface interacts with light (reflectance and scattering) described by sun-sensor viewing geometry and accounted by the bidirectional reflectance distribution function (BRDF) [31]. In this study, it is affected by a complex mixture of variables, including crown/canopy shape/structure, species composition, partial crown transparency, leaf orientation, and shadows. Consequently, the tree species used in this study were arranged in the following order according to the obtained canopy height accuracy (from worst to high): pine, spruce, birch, and black alder (Figure 7).

A tapering ovoid shape characterises the pine with an average crown diameter of around four meters, branchless for most of the trunk length. Furthermore, it does not have dense foliage (relatively transparent) with upward-pointing branches at the top of the crown, influencing light scattering **(**Figure 9a). Consequently, the matching could not detect the top of the trees, provided median −1.5 m canopy height underestimation with satellite (GE1) and even −1.2 m with airborne UltraCAM (Figure 7), which makes up about 6–7% of average canopy height. Moreover, due to the *pines*' scattered reflectance and non-uniformity at the tops of the crowns, altogether with a high B/H ratio, the Pleiades-based models have shown unsatisfactory results in pine canopy detection (73%) and height underestimation (~−2 m).

In turn, the *Norway spruce* (Figure 9b), with the classic conic shape and needle-like leaves that grow around the upward-pointing branches, is non-transparent for sunlight. As a result, spruce has a very high (>99.5%) detection rate, but due to the sharp and narrow treetop, the canopy height underestimation is still high~−1 m for satellite (GE1) sensors. Interestingly, in the *spruce* canopy height estimation, the highest difference between satellite and airborne DSM results was obtained among the rest tree species. UltraCam showed twice better results than the best GE1 image-based model (−0.5 m against −1 m GE1). According to Liang and Matikainen (2007) [34], it can be inferred that for a cone-shaped spruce crown, the lower and upper crown parts can fall into the same raster cell. Thus, thanks to the better imagery resolution (0.25 vs 0.5m in GE1), the UltraCAM model has shown significant improvement in *spruce* canopy height estimation.

Deciduous birch (*Betula pendula*) trees (Figure 9c) have main branches upward, with pendulous thin branches forming a "loose" crown, often with multiple peaks and changeful crown width and shape. The *birch* canopy height estimation is much better than coniferous *pine* and *spruce* tree species but still negative~−0.25 m for all image-based DSM models (except Pleiades −0.50 m). Matured broadleaf *black alder* (Figure 9d) trees with one or more trunks develop an arched, dense, and gently sloping crown shape opaque to light. It provides the best results in canopy height estimation, close to zero with the highest (99.9%) canopy detection rate. The structure of the crown of *black alder* also contributes to acceptable performance for satellite imagery obtained with a high base-to-ratio parameter (Pleiades case).

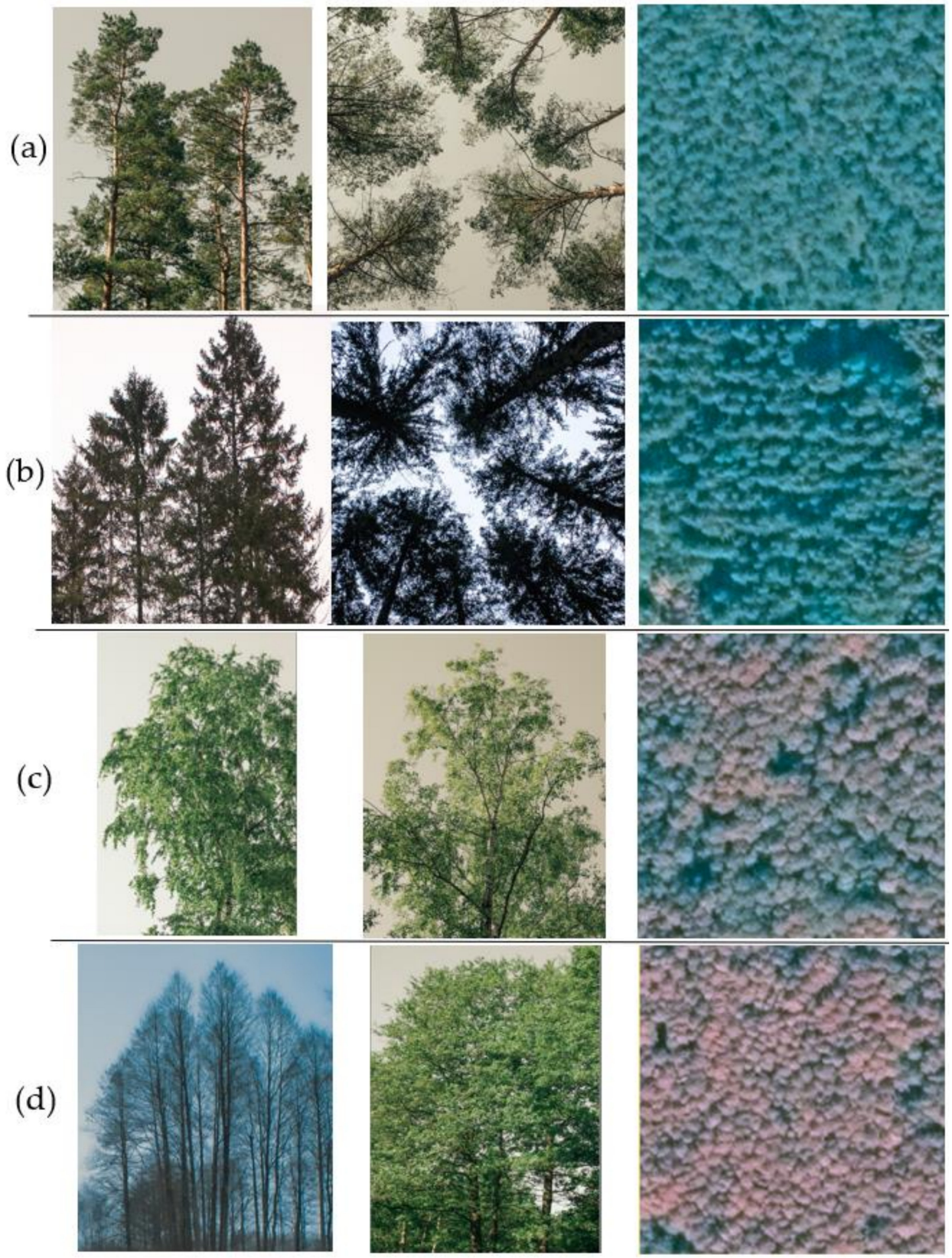

Figure 9. The four selected tree species of this study, (**a**) pine *(Pinus sylvestris)*, (**b**) spruce (*Pícea ábies*), both with vertical canopy profile and zenith views, (**c**) birch (*Bétula*), vertical canopy profile and oblique shot, (**d**) black alder (*Álnus glutinósa*), vertical canopy profile leaf-off and leaf-on shots. The third column—GE1 backscattered imagery NIR-G-B fragments (1 ha) of related tree species in the study area.

5.4. Spectral Band Performance of Satellite Image-Based DSMs

Overall, the current study found minor differences in image-based DSM performance related to spectral band imagery selection among the four tree species used (Figure 6). In the GE1 case, the highest canopy height accuracy was achieved using PAN and BLUE bands, and the worst when using NIR or RED ones. In all cases, the spread of median error between the best and worst model did not exceed 10%, at the same time showing almost identical results in error distribution and completeness. No significant differences were found between Pleiades and GE1 image-based DSMs, except the *pine* case. The discrepancy between the NIR and RED Pleiades image-based DSMs achieved 12% in *pine* detection (completeness) and showed the 0.5 m shift of mean error.

One significant and unanticipated finding was that GeoEye1 BLUE-based DSMs showed the best performance in canopy height estimation for all tree species, including deciduous. At the same time, the NIR and RED band-based DSMs were the worst, regardless of tree species. This finding was unexpected because vegetation spectra dominated by chlorophyll have the highest reflection in the NIR/RED [35]. The author's recent research [28] in Australian savannas showed that near-infrared BRDF, which is sensitive to canopy cover with higher contrast between canopy and the bare ground surface, provides the best efficiency in sparse *Eucalypt* vegetation detection. It seems that in cases where the ground surface is fully covered by dense closed-canopy forest, the NIR/RED resulted in insufficient local image contrast between the sunlit top of the crowns and surrounding shadows for improved canopy detection.

These results agree with other studies' findings [36] that outlined the importance of the BLUE channel for forest species pixel-based classification and coniferous tree species discrimination. Immitzer et al. (2016) demonstrated the importance of the blue band for vegetation mapping using the Random Forest model, emphasising the weakness of near-infrared spectral information. Unfortunately, the conformation to study findings related to high BLUE band performance for canopy height detection using stereo-satellite imagery has not been found in literature. Thus, this could be an essential issue for future research.

The discrepancy between the best-performed BLUE (GeoEye1) and GREEN (Pleiades) image-based DSM models could be attributed to the pre-defined spectral ranges of a BLUE band in given satellites: GeoEye1 450–510, Pleiades 430–550 nm. Therefore, based on its spectrum, the Pleiades BLUE channel corresponds more to the BLUE-GREEN range. In summary, considering that the difference in canopy height estimation between the PAN and pan-sharpened spectral models was minimal (GeoEye), this study recommends using a high-resolution stereo PAN band for DSM calculations in closed-canopy *hemiboreal* forest areas.

5.5. Aspects, Limitations and Recommendations for Data Processing by Stereo Satellites

This research has shown that determining the optimum B/H ratio is critical for the efficiency of image-based DSM in dense, closed-canopy forests. As the B/H ratio increases, the number of pixels comprising the canopy surface decreases due to insufficient reflation and occlusions, with the likelihood that neighbouring pixel similarity also decreases. Due to the conical crown structure of coniferous tree species and relative transparency (*pine* case) affecting the BRDF, a high satellite sensor B/H ratio can lead to relatively poor image-matching results (Pleiades case). In its turn, decreasing the number of potential pixel matches reduces the ability to estimate the object surface or canopy height correctly. The study results should be interpreted cautiously, as the current research has only examined the *hemiboreal* dense, close-canopy forest areas. The canopy height underestimation of satellite image-based DSMs has to be considered when derived information will be used for further calculations of the forest inventory parameters. Thus, further research needs to be conducted to validate a B/H ratio performance for other vegetation types with varied canopy densities and located in different geographical regions.

This research has several practical applications to be applied in dense Latvian forests. Although LiDAR data provide higher tree detection rates and more accurate canopy height

estimates, the spatial coverage and temporal resolution are limited due to the cost and time needed for data acquisition. Thereby, this increases the need for a regular flow of optical data acquired by national mapping agencies to support AGB mapping, forest inventory, and monitoring. In Latvia, a three-year cycle of collecting airborne imagery (0.25 m GSD) is used to perform complete territory mapping (orthophoto). This study showed that large-format aerial photography (e.g., UltraCam) is the optimal solution for creating the most accurate image-based DSM in vast and dense forestland. However, even such a short aerial photography cycle is not enough to quickly register and respond to all changes in vegetation. This study confirmed that satellite-based image matching (with optimal B/H ratio) is an adequate low-cost alternative for detecting canopies in *hemiboreal* forest areas with over 98% canopy detection rate and sufficient canopy height estimation accuracy (NMAD < 2 m). However, compared to LiDAR, optical sensors are strongly influenced by solar illumination, sun-to-sensor and sensor-to-target geometry (i.e., BRDF). In Latvian conditions, it is vital to remember that the insufficient sunlight during the winter season, and summer season clouds, sometimes restrict the use of satellite sensors, making image-based vegetation monitoring problematic.

One surprising finding was related to the indirect link between the human eyes performance of manual stereo data restitution and the computer vision matching technique. In most cases, the better and more accurately the human eyes can identify/detect a canopy by using stereo vision, the higher performance of image matching will be attained. This rule is correct for both sensor-to-target and sun-to-sensor geometry differences. It was especially noticeable during manual stereo comparison of different spectral GE1 and Pleiades imagery pairs. Thus, most likely that an experienced operator using a manual visual stereo check can filter and select the proper stereo imagery pairs for further use in image matching.

6. Conclusions

In this investigation, the main aim was to assess airborne and VHRSI satellite image-based DSM performance for canopy height estimation in predominantly mature, dense, closed-canopy Latvian *hemiboreal* forestland. Although airborne-based DSMs showed the highest efficiency, this study confirmed that commercially available VHRSI imagery could be a suitable and accurate alternative for detection and estimating canopy height in dense, closed-canopy forests. The canopy detection rates (completeness) by using GeoEye1 stereo imagery varied from 98% (*pine*) to >99% for *spruce* and deciduous tree species.

After performing a direct comparison of calculated image-based DSM models with reference LiDAR, the study confirmed the tendency for canopy height underestimation for all satellite-based models. The obtained accuracy of the canopy height estimation GE1-based models varied as follows: for a *pine* (−1.49 median, 1.52 m NMAD), *spruce* (−0.94 median, 1.97 m NMAD), *birch* (−0.26 median, 1.96 m NMAD), and *black alder* (−0.31 median, 1.52 m NMAD).

The significant finding was that the base-to-height ratio (convergence angle), a part of sensor-to-target geometry, is critical for canopy height estimation efficiency and completeness using image-based DSMs. Thus, this study suggests that stereo imagery with a B/H ratio range of 0.2–0.3 (or convergence angle range 10–15°) is optimal for image-based DSMs in closed-canopy forest areas. Furthermore, besides the B/H ratio, the study confirmed that the canopy height estimation efficiency is affected by a complex mixture of variables, including crown/canopy shape/structure, species composition, partial crown transparency, leaf orientation, and shadows. Finally, this study has found that, generally, the spectral bands of VHRSI imagery have a minor impact on canopy detection rates and canopy height estimation accuracy in dense, closed-canopy *hemiboreal* forestland. Therefore, in most cases, the study recommends using a satellite high-resolution stereo PAN band for DSM generation.

Funding: The financial support for this work was provided to the Institute of Electronics and Computer Science (Latvia) by the European Regional Development Fund (ERDF) within a funded project entitled "Satellite remote sensing-based forest stock estimation technology" (grant number No. 1.1.1.1/18/A/165).

Institutional Review Board Statement: Not applicable.

Informed Consent Statement: Not applicable.

Data Availability Statement: The study did not report any data.

Acknowledgments: This work was supported by the Latvian Institute of Electronics and Computer Science (EDI) whose staff are gratefully thanked for their assistance. Forest inventory data for this study was provided by the JSC Latvia's State forests. Latvian Geospatial Information Agency (LGIA) supported this work by providing LiDAR and airborne imagery data, to whose staff I would like to express my gratitude for their cooperation. The author wishes to express his thanks to Victor Adrov (JSC Racurs) for technical support. Additionally, above all, I dedicate this work in memory of my mentor Jānis Klētnieks (1929–2021), great Latvian surveyor and photogrammetrist.

Conflicts of Interest: The author declares no conflict of interest. The funders had no role in the study's design; in the collection, analyses, or interpretation of data, in the writing of the manuscript, or in the decision to publish the results.

References

1. Young, R.A.; Giese, R.L. (Eds.) *Introduction to Forest Ecosystem Science and Management*, 3rd ed.; Wiley: Hoboken, NJ, USA, 2003; ISBN 978-0-471-33145-2.
2. Trumbore, S.E.; Brando, P.; Hartmann, H. Forest health and global change. *Science* **2015**, *349*, 814–818. [CrossRef] [PubMed]
3. Lazdiņš, A. *Latvia' S National Forestry Accounting Plan and Proposed Forest Reference Level 2021–2025*; LSFRI Silava: Salaspils, Latvia, 2019; p. 68.
4. Franklin, S.E. *Remote Sensing for Sustainable Forest Management*; CRC Press: Boca Raton, FL, USA, 2001; ISBN 9781566703949.
5. Fang, J.; Brown, S.; Tang, Y.; Nabuurs, G.-J.; Wang, X.; Shen, H. Overestimated Biomass Carbon Pools of the Northern mid- and High Latitude Forests. *Clim. Chang.* **2006**, *74*, 355–368. [CrossRef]
6. Maltamo, M.; Næsset, E.; Vauhkonen, J. *Forestry Applications of Airborne Laser Scanning: Concepts and Case Studies*; Springer: Berlin/Heidelberg, Germany, 2014; Volume 27, ISBN 978-94-017-8663-8.
7. Hyyppä, J.; Hyyppä, H.; Leckie, D.; Gougeon, F.; Yu, X.; Maltamo, M. Review of methods of small-footprint airborne laser scanning for extracting forest inventory data in boreal forests. *Int. J. Remote Sens.* **2008**, *29*, 1339–1366. [CrossRef]
8. Immitzer, M.; Stepper, C.; Böck, S.; Straub, C.; Atzberger, C. Use of WorldView-2 stereo imagery and National Forest Inventory data for wall-to-wall mapping of growing stock. *For. Ecol. Manag.* **2016**, *359*, 232–246. [CrossRef]
9. White, J.C.; Wulder, M.A.; Vastaranta, M.; Coops, N.C.; Pitt, D.; Woods, M. The Utility of Image-Based Point Clouds for Forest Inventory: A Comparison with Airborne Laser Scanning. *Forests* **2013**, *4*, 518–536. [CrossRef]
10. Hirschmuller, H. Stereo Processing by Semiglobal Matching and Mutual Information. *IEEE Trans. Pattern Anal. Mach. Intell.* **2007**, *30*, 328–341. [CrossRef]
11. Ahmadabadian, A.H.; Robson, S.; Boehm, J.; Shortis, M.; Wenzel, K.; Fritsch, D. A comparison of dense matching algorithms for scaled surface reconstruction using stereo camera rigs. *ISPRS J. Photogramm. Remote. Sens.* **2013**, *78*, 157–167. [CrossRef]
12. Pearse, G.D.; Dash, J.P.; Persson, H.J.; Watt, M.S. Comparison of high-density LiDAR and satellite photogrammetry for forest inventory. *ISPRS J. Photogramm. Remote. Sens.* **2018**, *142*, 257–267. [CrossRef]
13. Piermattei, L.; Marty, M.; Ginzler, C.; Pöchtrager, M.; Karel, W.; Ressl, C.; Pfeifer, N.; Hollaus, M. Pléiades satellite images for deriving forest metrics in the Alpine region. *Int. J. Appl. Earth Obs. Geoinf.* **2019**, *80*, 240–256. [CrossRef]
14. Neigh, C.S.R.; Masek, J.G.; Bourget, P.; Cook, B.; Huang, C.; Rishmawi, K.; Zhao, F. Deciphering the Precision of Stereo IKONOS Canopy Height Models for US Forests with G-LiHT Airborne LiDAR. *Remote. Sens.* **2014**, *6*, 1762–1782. [CrossRef]
15. St-Onge, B.; Grandin, S. Estimating the Height and Basal Area at Individual Tree and Plot Levels in Canadian Subarctic Lichen Woodlands Using Stereo WorldView-3 Images. *Remote. Sens.* **2019**, *11*, 248. [CrossRef]
16. Persson, H.J.; Perko, R. Assessment of boreal forest height from WorldView-2 satellite stereo images. *Remote Sens. Lett.* **2016**, *7*, 1150–1159. [CrossRef]
17. Ullah, S.; Dees, M.; Datta, P.; Adler, P.; Saeed, T.; Khan, M.S.; Koch, B. Comparing the potential of stereo aerial photographs, stereo very high-resolution satellite images, and TanDEM-X for estimating forest height. *Int. J. Remote. Sens.* **2020**, *41*, 6976–6992. [CrossRef]
18. Fassnacht, F.E.; Mangold, D.; Schäfer, J.; Immitzer, M.; Kattenborn, T.; Koch, B.; Latifi, H. Estimating stand density, biomass and tree species from very high resolution stereo-imagery—Towards an all-in-one sensor for forestry applications? *Forestry* **2017**, *90*, 613–631. [CrossRef]

19. McGaughey, R.J. *FUSION/LDV: Software for LiDAR Data Analysis and Visualization—V4.20*; USDA For. Serv.: Washington, DC, USA, 2021.
20. Conrad, O.; Bechtel, B.; Bock, M.; Dietrich, H.; Fischer, E.; Gerlitz, L.; Wehberg, J.; Wichmann, V.; Böhner, J. System for Automated Geoscientific Analyses (SAGA) v. 2.1.4. *Geosci. Model Dev.* **2015**, *8*, 1991–2007. [CrossRef]
21. QGIS. QGIS Geographic Information System. Open Source Geospatial Foundation Project. Available online: http://www.qgis.org (accessed on 1 February 2021).
22. Grodecki, J.; Dial, G. Block Adjustment of High-Resolution Satellite Images Described by Rational Polynomials. *Photogramm. Eng. Remote Sens.* **2003**, *69*, 59–68. [CrossRef]
23. Mutluoglu, O.; Yakar, M.; Yilmaz, H.M. Investigation of effect of the number of ground control points and distribution on adjustment at WorldView-2 Stereo images. *Int. J. Appl. Math. Electron. Comput.* **2014**, *3*, 37. [CrossRef]
24. Meguro, Y.; Fraser, C.S. Georeferencing accuracy of GeoEye-1 stereo imagery: Experiences in a Japanese test field. *Int. Arch. Photogramm. Remote Sens. Spat. Inf. Sci.* **2010**, *38*, 1069–1072.
25. Donis, J. *Creation of the Scientific Substantiation for an Information Updating in the Forest State Register*; Latvian State Forest Research Institute Silava: Salaspils, Latvia, 2014.
26. Höhle, J.; Höhle, M. Accuracy assessment of digital elevation models by means of robust statistical methods. *ISPRS J. Photogramm. Remote Sens.* **2009**, *64*, 398–406. [CrossRef]
27. Aguilar, M.A.; Saldana, M.D.M.; Aguilar, F.J. Generation and Quality Assessment of Stereo-Extracted DSM from GeoEye-1 and WorldView-2 Imagery. *IEEE Trans. Geosci. Remote Sens.* **2013**, *52*, 1259–1271. [CrossRef]
28. Goldbergs, G.; Maier, S.W.; Levick, S.R.; Edwards, A. Limitations of high resolution satellite stereo imagery for estimating canopy height in Australian tropical savannas. *Int. J. Appl. Earth Obs. Geoinf.* **2019**, *75*, 83–95. [CrossRef]
29. Jeong, J.; Kim, T. Quantitative Estimation and Validation of the Effects of the Convergence, Bisector Elevation, and Asymmetry Angles on the Positioning Accuracies of Satellite Stereo Pairs. *Photogramm. Eng. Remote Sens.* **2016**, *82*, 625–633. [CrossRef]
30. Hasegawa, H.; Matsuo, K.; Koarai, M.; Watanabe, N.; Masaharu, H. DEM Accuracy and the Base to Height (B/H) Ratio of Stereo Images. *Int. Arch. Photogramm. Remote Sens.* **2000**, *33*, 356–359.
31. Gerard, F.; North, P. Analyzing the effect of structural variability and canopy gaps on forest BRDF using a geometric-optical model. *Remote Sens. Environ.* **1997**, *62*, 46–62. [CrossRef]
32. Straub, C.; Tian, J.; Seitz, R.; Reinartz, P. Assessment of Cartosat-1 and WorldView-2 stereo imagery in combination with a LiDAR-DTM for timber volume estimation in a highly structured forest in Germany. *Forestry* **2013**, *86*, 463–473. [CrossRef]
33. Qin, R. A critical analysis of satellite stereo pairs for digital surface model generation and a matching quality prediction model. *ISPRS J. Photogramm. Remote Sens.* **2019**, *154*, 139–150. [CrossRef]
34. Liang, X.; Matikainen, L. Deciduous-Coniferous Tree Classification Using Difference Between First and Last Pulse Laser Signatures. *ISPRS* **2007**, *36*, 253–257.
35. Immitzer, M.; Atzberger, C.; Koukal, T. Tree Species Classification with Random Forest Using Very High Spatial Resolution 8-Band WorldView-2 Satellite Data. *Remote Sens.* **2012**, *4*, 2661–2693. [CrossRef]
36. Fassnacht, F.; Latifi, H.; Stereńczak, K.; Modzelewska, A.; Lefsky, M.; Waser, L.; Straub, C.; Ghosh, A. Review of studies on tree species classification from remotely sensed data. *Remote Sens. Environ.* **2016**, *186*, 64–87. [CrossRef]